Tuning Flame Spray Pyrolysis for Variation of the Crystallite Size in Cu/ZnO/ZrO_2 and its Influence on the Performance in CO_2-to-Methanol Synthesis

Mariam L. Schulte,[a, b] V. Catharina Sender,[a, b] Lorena Baumgarten,[a, b] Arik Beck,[a] Ajai R. Lakshmi Nilayam,[c] Erisa Saraçi,[a, b] and Jan-Dierk Grunwaldt*[a, b]

CO_2 hydrogenation to methanol (MeOH) is a key transformation in the Power-to-liquid concept, which aims to store energy in chemical energy carriers and chemicals. Cu/ZnO/ZrO_2 (CZZ) shows great promise due to its enhanced stability in the presence of water, a critical by-product when utilizing CO_2-based feedstocks. The structure-sensitivity of this reaction, especially for particle sizes below 10 nm and in three-component systems, remains highly debated. Herein, we systematically prepared a series of CZZ catalysts by flame spray pyrolysis (FSP) to vary the crystallite size and to study its effect on methanol synthesis in this three-component system. FSP enabled us to maintain a fixed Cu/Zn/Zr ratio close to the commercial composition (61/29/10 atomic ratio), while varying the precursor feed rate. This resulted in variation in the crystallinity. The characterization by X-ray diffraction and electron microscopy revealed an increase in crystallite size with rising feed rate for Cu and t-ZrO_2, whereas ZnO remained mostly unaffected. The testing of the materials in methanol synthesis uncovered an increase in performance, higher space time yield and MeOH selectivity, with decreasing crystallite size for two (Cu, t-ZrO_2) of its three components. The increased selectivity with smaller sizes might be attributed to an increase in interfacial sites.

Introduction

The conversion of green hydrogen and CO_2 to form liquid energy carriers, also known as Power-to-liquid (PtL) concept, has garnered significant attention in recent years.[1] In this approach, energy produced from renewable sources is converted into synthetic fuels and base chemicals, such as methanol (MeOH), dimethylether (DME) or hydrocarbons, which serve as substitutes for fossil resources.[2] MeOH, in particular, is a promising candidate due to its high energy density, its role as a platform molecule for various chemicals, (*e.g.*, acetic acid, propylene or DME), and its existing large volume market.[3] Conventionally, MeOH is produced by syngas (CO/H_2) with small amounts of CO_2 using a Cu/ZnO/Al_2O_3 (CZA) catalyst[4] under reaction conditions of 50–100 bar and 200–300 °C.[5] CO and CO_2 hydrogenation to MeOH (eq. 1 and 2) are exothermic and favored at lower temperatures. However, due to kinetic limitations the reaction has to be performed at elevated temperatures and active catalysts are required.[6]

$$CO + 2\ H_2 \rightarrow\ CH_3OH \qquad \Delta H_{298K}\ =\ -90.6\frac{kJ}{mol} \tag{1}$$

$$CO_2 + 3\ H_2 \rightarrow\ CH_3OH +\ H_2O \qquad \Delta H_{298K}\ =\ -49.5\frac{kJ}{mol} \tag{2}$$

The hydrogenation of CO_2 to MeOH, presents new challenges when compared to conventional MeOH synthesis from syngas. The less favorable thermodynamics of the CO_2-based feed leads to a maximum equilibrium MeOH yield of 18–58 % (at 200 °C and 50–100 bar), which is substantially lower than 55–89 % yield achievable with CO-based feed.[1] Furthermore, the large water amount formed in the reaction (eq. 2) accelerates the deactivation of the CZA catalyst due to the growth of Cu and ZnO crystallites.[7] The utilization of ZrO_2, which has less hydrophilic properties compared to Al_2O_3, is well established and a higher tolerance against water-induced deactivation is claimed.[8] A deactivation study on a Cu/ZnO/ZrO_2 (CZZ) catalyst identified Cu crystallite growth and ZnO restructuring as main reasons for activity loss.[9] However, the role of each component in this active and selective ternary CZZ catalyst system remains a topic of debate. A key question concerns the structure-sensitivity of the reaction: How particle size, orientation, and shape influence catalytic performance. Studying particle size influences for

[a] M. L. Schulte, V. Catharina Sender, L. Baumgarten, A. Beck, E. Saraçi, J.-D. Grunwaldt
Institute for Chemical Technology and Polymer Chemistry, Karlsruhe Institute of Technology, Engesserstr. 20, 76131 Karlsruhe, Germany
E-mail: grunwaldt@kit.edu

[b] M. L. Schulte, V. Catharina Sender, L. Baumgarten, E. Saraçi, J.-D. Grunwaldt
Institute of Catalysis Research and Technology, Karlsruhe Institute of Technology, Hermann-von-Helmholtz Platz 1, 76344 Eggenstein-Leopoldshafen, Germany

[c] A. R. L. Nilayam
Karlsruhe Nano Micro Facility (KNMFi), Karlsruhe Institute of Technology, Hermann-von-Helmholtz Platz 1, 76344 Eggenstein-Leopoldshafen, Germany

MeOH synthesis in this catalytic system must meet certain criteria to yield relevant insights into industrially relevant catalyst structures.[10] Most importantly, the elemental composition of the established CZA and CZZ systems closely adheres to the ≈60% Cu content, with Al_2O_3 or ZrO_2 comprising only a minor fraction of the catalyst.[11] Furthermore, the distributions of the components has to be in close contact, since this is one of the most crucial requirements for high activity and selectivity.[12] Designing catalyst samples to investigate structure-sensitivity in CZZ catalysts is, therefore, challenging, since conventional synthesis methods for varying particle size, *e.g.*, (incipient) wetness impregnation, cannot meet the aforementioned criteria.

Flame spray pyrolysis (FSP) offers a viable synthesis method, which is fast and reproducible.[13] It allows precise tuning of particle size, crystallinity, and morphology by varying different parameters, such as precursor feed rate, solvent, and concentration.[14] This method was employed to prepare highly active binary systems and ternary systems (Cu–Zn based) for MeOH and DME synthesis.[15] However, these catalysts often have particle sizes exceeding 10 nm. Structure-sensitivity of the CO-to-methanol reaction was found for Cu particles below 8 nm,[16] whereas for CO_2 hydrogenation contradicting results were reported, probably due to variations in reaction conditions, catalyst compositions and supports used in different studies.[17] Some studies reported an increase in activity with increase in particle size,[8a,18] in contrast to investigations that found smaller particles are beneficial and lead to a higher active surface area.[19] Therefore, there is a need to expose particle size dependencies, especially below 10 nm, using catalyst samples, that closely resemble industrially relevant structures and compositions.

Here, we aim to investigate the influence of FSP parameters on the catalyst structure of the three different components in CZZ catalysts with compositions close to those used industrially. By varying the FSP feed rate during synthesis procedure and by using the three-component system, we were able to vary the crystallite sizes (3.5–6 nm), while maintaining a constant Cu/Zn/Zr ratio across all catalysts. As next step the correlation of the chemical/structural properties (as determined by H_2-TPR, N_2O-titration, XRD, BET, ICP-OES, TGA, and TEM) with the catalytic activity and selectivity in CO_2-to-MeOH synthesis was explored. In this way, we aimed at investigating the influence of different crystallite sizes of all three components, resulting from FSP parameter variation, on the performance in CO_2-based MeOH synthesis.

Results and Discussion

Catalyst Synthesis and Composition

A series of CZZ catalysts were prepared by FSP using different feed rates ranging from 3 mL/min to 12 mL/min. An increase in feed rate leads to more solvent combusted in the flame resulting in a larger flame and higher combustion enthalpy (as seen from right to left in Figure 1). In a larger flame the particles

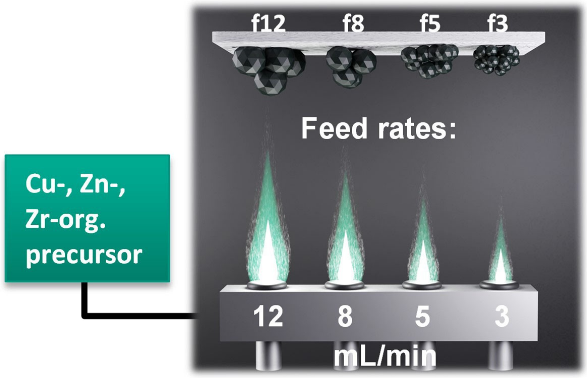

Figure 1. Scheme of flame spray pyrolysis synthesis with varying precursor feed rate and the influence on particle size.

have more time to agglomerate leading to a particle size increase and more crystalline phases.[20] In order to form homogeneous particles via the gas-to-particle mechanism, the combustion enthalpy density should be above 4.7 kJ/g_{gas}.[20b] For all prepared catalysts, these requirements are fulfilled (Table S2–S3, eq. S1, ESI). The as-prepared batches were split in half. One half was kept as is and the other half was subsequently calcined at 300 °C to investigate possible organic residues. The catalysts are named according to the used feed rate and calcination state *e.g.* f8 was sprayed using an 8 mL/min flow without calcination and f12-calc was sprayed with a 12 mL/min flow and calcined at 300 °C.

The as-prepared catalysts were characterized by several methods to gain insight to the catalyst composition (ICP-OES), remaining organic residues (TGA), crystal structure and crystallite size (XRD), distribution (STEM-EDX) as well as morphology and particle size (TEM). The results are summarized in Figure 2. All catalysts have a similar composition of 43 ± 1 wt.% Cu, 21 ± 1 wt.% Zn and 10 ± 0.5 wt.% Zr, with the exception for catalyst f3 which consists of 39 ± 1 wt.% Cu, 19 ± 1 wt.% Zn and 9 ± 0.5 wt.% Zr. The oxygen content was calculated according to the metal amount (Table S6, ESI). The remaining residues vary between 5–8 wt.% which could be due to moisture and/or carbonates on the surface. For f3 remaining residues of 15 wt.% indicate an incomplete combustion and remaining organic residues in the catalyst. The calculated ratio of Cu/Zn/Zr for all catalysts was 61/29/10, which is close to the intended ratio of 60/30/10. This ratio was chosen since ternary CZZ catalysts with similar composition exhibited high activity in CO_2-to-MeOH synthesis.[21] After calcination at 300 °C, the composition of f5-calc to f12-calc is similar to the uncalcined (f5-f12) samples. For f3, an increase from 39 wt.% to 42 wt.% for Cu, 19 wt.% to 21 wt.% for Zn, and 9 wt.% to 10 wt.% for Zr was observed, supporting the speculation that organic residues are present and decompose below 300 °C for this sample.

The removal of residues was analyzed in more detail by thermogravimetric analysis (TGA) in static synthetic air. All catalysts, except for f3, show a weight loss of 4–6% in a temperature range from 25 °C to 800 °C as shown in Figure 2a. After 300 °C, only 1% weight loss is detected until 800 °C. Since

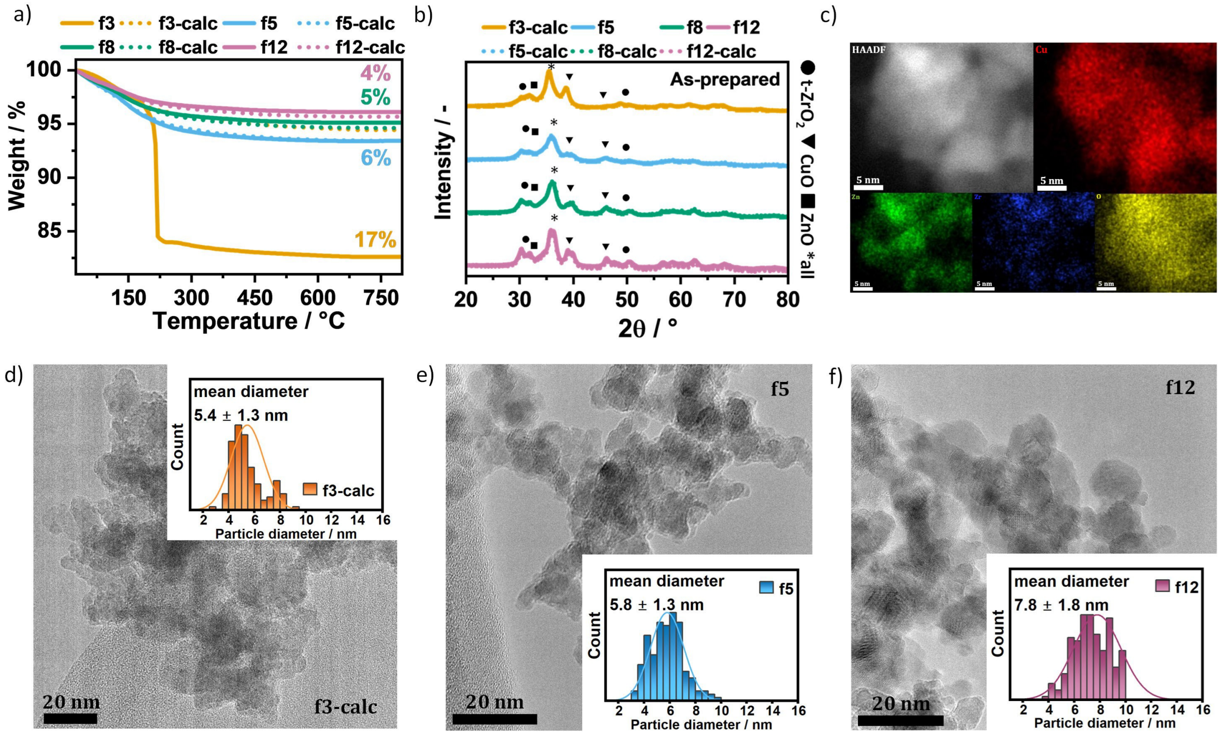

Figure 2. a) Weight loss as function of temperature determined by thermal gravimetric analysis of the as prepared catalysts b) X-ray diffraction patterns of as-prepared catalysts c) HAADF-STEM image of the as-prepared f3-calc catalyst with EDX mapping of Cu (red), Zn (green), O (yellow) and Zr (blue) d–f) TEM images of the catalysts f3-calc (d), f5 (e) and f12 (f) with particle size distribution of each catalyst obtained by particle counting.

calcined and uncalcined catalysts (feed rate 5–12 ml/min) show a similar behavior, the presence of residues due to the synthesis methods can be excluded under these preparation conditions. Catalyst f3 shows a weight loss of total 17% over the complete temperature range with the major losses occurring below 300°C. This further supports the conclusion that for this sample uncombusted residues from the synthesis are present due to the low combustion enthalpy and small flame. These residues influence the surface and catalytic properties, and their amount and nature of those residues will change during the catalytic process. This prevents a correlation of observed performance with structure through *ex-situ* characterization for this catalyst. Therefore, the catalyst f3 has been excluded from further discussions and the results can be found in ESI.

The crystal structure of the as-prepared catalysts was investigated with XRD. In Figure 2b, the diffraction patterns show broad reflections indicating small crystallite sizes and, also, the presence of X-ray amorphous species. CuO, ZnO and tetragonal ZrO_2 (t-ZrO_2) phases were detected with no other detectable ZrO_2 phases. The presence of t-ZrO_2 is in line with other synthesized ZrO_2 containing solid materials by FSP.[15b,f,h,22]. The main reflections of t-ZrO_2 can be found at 30.2° (111) and 50.2–50.8° (220/400). The incorporation of Cu or Zn into the ZrO_2 lattice would lead to distortion and result in a shift of the (111) reflection.[15b,23] Since for all catalysts the reflection (ZrO_2, 111) is located at 30.2°, the incorporation of Cu and Zn ions in the ZrO_2 lattice may have only happened to a small, undetectable extent, if at all. In the range from 34.5° to 36.5° all components have overlapping reflections: 34.5° and 36.3° for ZnO, 35.6° for CuO and 34.6° and 35.3° for t-ZrO_2. The main reflection of CuO is found at 38.8° (double peak) and 48.8°. ZnO has a main reflection at 31.8°. With increasing feed rate from f5 to f12 the reflections get sharper and more pronounced indicating an increase in crystallite size and crystallinity due to the longer residence time in the flame. For the samples prepared at feed rates above 5 mL/min feed rate, no significant changes can be seen in the XRD patterns after calcination, which agrees with TGA results. For catalyst f3-calc, the CuO reflection at 48.8° is sharper than for f5 and f8. This indicates CuO agglomeration caused by the calcination and removal of organic residues. Due to the nanocrystalline nature of the materials meaningful Rietveld refinements of the oxidized catalyst samples were not possible.

The spatial distribution of Cu, Zn, and Zr was investigated by STEM-EDX for sample f3, f3-calc, f5 and f12. The presence of CuO, ZnO and ZrO_2 in close contact in f3-calc sample is shown in Figure 2c and was also true for the other investigated catalysts (Figure S1, ESI). Furthermore, particle size distribution was determined by particle counting for catalyst f3-calc, f5 and f12 (Figure 2d–f, see sample f3 in Figure S1d, ESI). The particle size distribution analysis from TEM images does not take into consideration the chemical composition of the individual catalyst particles. The results confirm XRD analysis observations, indicating that particle size increase with increasing feed rate from 5.4±1.3 nm to 7.8±1.8 nm. Note that these nanoparticles aggregate into larger ones in all cases, but in the crystalline structure of the 5–8 nm large nanoparticle is clearly visible in the TEM images.

Reducibility and Surface Properties

The reducibility and surface properties were investigated and summarized in Figure 3 and Table S7, ESI. The reduction behavior of the catalyst series was examined using H_2-temperature-programmed reduction (H_2-TPR). During H_2-TPR a broad H_2 consumption peak between 140–160 °C was observed for all catalysts (Figure 3a) stemming from the reduction of Cu^{2+} to Cu^0.[24] Similar reduction temperatures were found for other CZZ catalysts.[8a,21d] The shoulders observed for some of the catalysts could be either due to the presence of two different Cu species[24] (finely dispersed CuO particles and larger bulk CuO), or due to temperature fluctuations during the H_2-TPR, where in case the sample sample temperature exceeds the setpoint, cooling is activated, leading to a shoulder. The latter mentioned behavior was observed in the temperature profiles which are shown in Figure S2, ESI.

After reduction, N_2O-titration was used to determine the active surface area (ASA). It is important to mention that this method is often employed to determine the Cu surface area.[8a,c,19,21c] However, it is worth noting that this method characterizes not only the Cu surface area, but also titrates oxygen vacancies in the ZnO and other oxides, even if performed at temperatures as low as 35 °C.[25] Therefore, this surface is called ASA and is considered to include Cu surface area and ZnO vacancies. For the catalyst series f5–f12, a decrease in ASA from 30 m^2/g to 22 m^2/g can be observed (Figure 3b). The catalyst f3-calc exhibited an ASA of 19 m^2/g. This is in line with the XRD observation of Cu agglomeration during the calcination process. Similar ASA were reported for CZZ catalysts prepared by continuous co-precipitation ranging from 10 to 27 m^2/g,[21d] and for a $Cu/ZnO/Al_2O_3$ catalyst prepared by FSP with 34 m^2/g.[15a] The overall surface area and pore volume of the as-prepared catalysts was investigated using N_2 physisorption (Table S7, ESI). For f5 to f12, a decrease in BET surface area from 110 m^2/g (f5) to 77 m^2/g (f12) and in the pore volume from 0.330 cm^3/g (f5) to 0.287 cm^3/g (f12) was observed. For f3-calc, a surface area of 99 m^2/g and a pore volume of 0.338 cm^3/g were observed. The samples prepared here, show structural properties in line with reported FSP and co-precipitated samples, validating the effectiveness of our approach in producing reliable catalysts with desirable structural characteristics.[8a,15g,21d]

The reduced and spent catalysts were examined with XRD and the reflection patterns are depicted in Figure S3, ESI. The main reflections of Cu can be found at $2\theta = 43.6°$ and overlapping with t-ZrO_2 at $2\theta = 50.9°$. For ZnO and t-ZrO_2, the same reflections as for the as-prepared samples can be detected. Furthermore, some CuO can also be identified, resulting from storing the samples under air prior the XRD measurements.[26] In comparison to the as-prepared state more pronounced reflections can be observed, which indicate agglomeration and crystallization during the reduction process. With Rietveld refinement, the crystallite sizes of all components were determined and displayed in Figure 3c (see details in Experimental section and ESI, Table S8–S14). For the catalysts f5–f12 an increase was observed in Cu crystallite size from 4.4 nm to 5.9 nm (blue bars) and also in t-ZrO_2 crystallite size from 2.6 nm to 4.6 nm (black bars). The trend is less pronounced for ZnO phases (orange bars). Interestingly Cu and t-ZrO_2 have similar size (3–6 nm), whereas ZnO is nearly 2 times larger (8–9 nm), with the exception for f3-calc which has a ZnO crystallite size of 4.2 nm. The Cu crystallite size of 5.5 nm for f3-calc is in line with the previous discussed ASA. A similar study varying the FSP feed rate with a Cu/ZrO_2 catalyst system obtained Cu crystallite sizes of 12–17 nm, which are significantly larger than in our study, probably due to the absence of ZnO, which improves the Cu dispersion.[15b] The variation in crystallite size of all three components within an industrially relevant range enables for the assessment of how the crystallite size influences catalytic performance.

Catalytic Performance

The catalyst series was tested for CO_2-to-MeOH synthesis at 40 bar and 235 °C with a ratio of H_2:CO_2 = 3 : 1. Besides CO (from reverse water gas shift reaction), there were no other side products detected. Three different weight hourly space velocities (WHSV = 75000, 37500, and 18750 mL/g_{cat}·h) were employed (summarized in Table S15–S17, ESI). Figure 4a shows the correlation of CO_2 conversion (X_{CO2}) to MeOH selectivity (S_{MeOH}) for all space velocities. The catalytic data from all tested

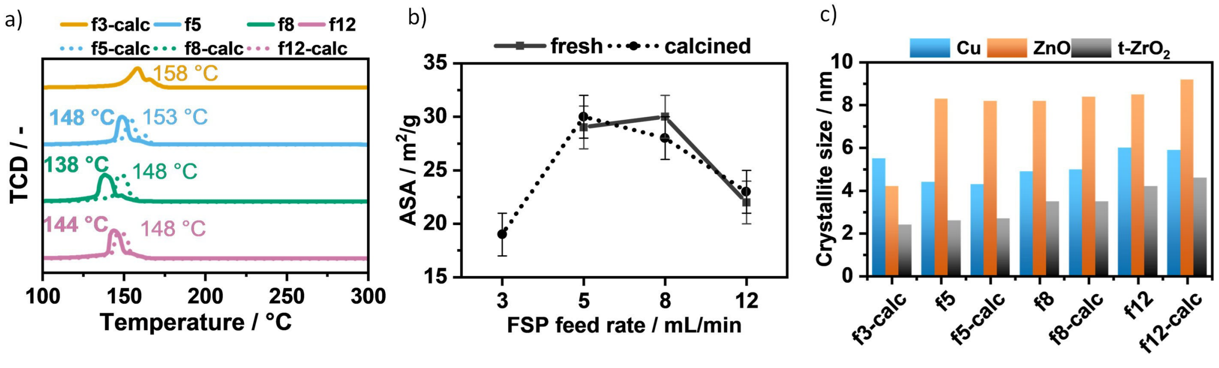

Figure 3. a) Reduction profiles obtained by H_2-TPR b) active surface area (ASA) obtained by N_2O-titration, error bars correspond to ± 2 m^2/g based on measurement of reference material c) crystallite sizes for Cu, ZnO and t-ZrO_2 obtained from Rietveld refinement of the spent catalysts.

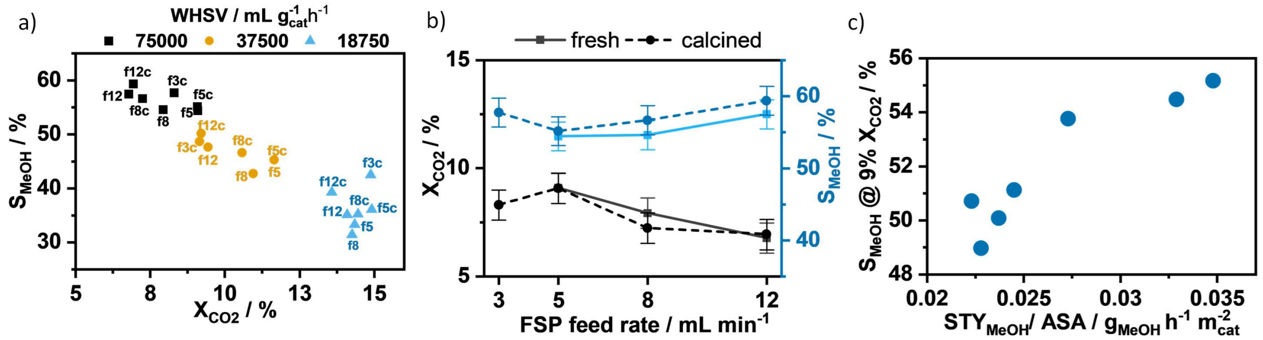

Figure 4. Catalytic activity of the catalyst series in CO_2 hydrogenation to MeOH at 40 bar and 235 °C a) MeOH selectivity (S_{MeOH}) plotted against CO_2 conversion (X_{CO2}) for all space time velocities b) X_{CO2} and S_{MeOH} at WHSV = 75 000 mL/g_{cat}·h with error bars for X_{CO2} of ±0.7 % and S_{MeOH} of ±2 % based on the deviation of f8 to f8-calc, which shows the maximum deviation of all samples c) MeOH selectivity at 9 % CO_2 conversion plotted against space time yield (STY) of MeOH normalized on ASA at 9 % CO_2 conversion.

samples fall on one linear correlation: The selectivity strongly decreases with increasing conversion (from 63 % S_{MeOH} at a X_{CO2} of around 7 % to 31 % S_{MeOH} at 15 % X_{CO2}). At high conversion levels, the linear trend is less pronounced. This could be due to near equilibrium conditions and undesired condensation of MeOH and H_2O. The shared overall trend in conversion-selectivity indicates that all the active centers of the catalyst series are part of the same family, which is expected due to the similar elemental composition and preparation method. The activity of catalyst series is comparable with a commercial CZA catalyst. Reported space time yields (STY) of CZA catalysts for CO_2-based feed under industrial conditions are in the order of 0.4–0.8 kg_{MeOH}/L_{cat}·h, which is comparable to the yields for this CZZ series, under similar conditions (high space velocities).[1]

Nevertheless, the samples showed performance differences, that are relevant for industrial applications and provide insights into the catalyst's structure-performance dependency. Figure 4b shows X_{CO2} and S_{MeOH} for all seven catalysts (WHSV = 75000), with MeOH yield detailed in Table S15. For f5–f12, X_{CO2} decreases from 9.1 % (f5) to 6.8 % (f12), alongside a small increase in S_{MeOH} from 55 % (f5) to 57 % (f12), leading to the overall trend (Figure 4a) of decreasing Y_{MeOH} from 4.9 % (f5) to 3.9 % (f12). Some of these performance differences may be directly attributed the conversion-selectivity dependence seen in Figure 4a. Therefore, for a better comparison, selectivity at 9 % iso-conversion (X_{CO2}) will be compared. The values for this conversion level were obtained through interpolation (Figure S4, ESI). At iso-conversion, methanol selectivity ranges from 48–55 % (Figure S5). For an industrial process, a selectivity change of 5 % can have a substantial impact on operation costs. To further investigate the intrinsic performance difference, we compared the STY at 9 % CO_2 conversion normalized to the obtained ASA (Figure S6, S7 and Table S18, ESI) with selectivity (Figure 4c). As stated above, the ASA includes Cu surface area and ZnO oxygen vacancies and will be used as descriptor for the active sites. Here, an overall trend of increasing selectivity with increasing STY can observed. This indicates that the more active catalyst is also more selective, which is a clear indication for a structure-sensitive reaction. Therefore, we turn to the structural information obtained from XRD.

Correlation of FSP Synthesis Parameters and Structural Properties with Catalytic Performance

XRD showed that the crystallite sizes of the three components evolve differently depending on the FSP synthesis conditions. By plotting the MeOH selectivity and STY normalized by ASA obtained at 9 % CO_2 conversion against the different crystallite sizes for Cu, ZnO and ZrO_2, we aim to disentangle the size effects (Figure 5). In Figure 5a and b, we examine the influence of the Cu crystallite size within a size range of 4–6 nm. A drop in activity for both MeOH and CO can be observed with increasing Cu crystallite size. However, the decrease is more pronounced for MeOH. This indicates that smaller Cu particles are more active and more selective towards MeOH. This can be confirmed when considering Figure 5b, which shows the selectivity towards MeOH plotted against the Cu crystallite size. However, the sample f8, with a Cu crystallite size of 4.9 nm is escaping the trend in STY and selectivity. Thus, while there might be a Cu size dependency favoring small Cu crystallites, this outlier weakens the correlation between Cu size and performance. The ZrO_2 crystallite size-performance dependency is shown in Figure 5c and d. Here, a more pronounced correlation in decreased performance for MeOH with increasing ZrO_2 crystallite size was found. Especially, considering the trends seen for MeOH selectivity in Figure 5d, a clear trend without outliers arises. Lastly, the ZnO crystallite size (Figure 5e and f) shows no correlation with activity or selectivity leading to the conclusion that their size has only a marginal influence on the catalytic performance.

Our findings show that CZZ catalysts are structure-sensitive in the industrially relevant composition range. However, these dependencies are difficult to disentangle due to the overlapping influences of the multi-component catalyst. Our series of flame-made CZZ catalysts showed that the chosen precursor feed rate influences surface areas (BET- and Cu surface + ZnO oxygen vacancies), pore volume, and overall particle sizes, which in turn influences catalytic performance: For our data, the best CZZ catalyst had small Cu crystallites (≈4 nm), large ZnO crystallites (≈8 nm) and small ZrO_2 crystallites (≈3 nm) (Figure 6). ZnO showed no size dependence, however the size was

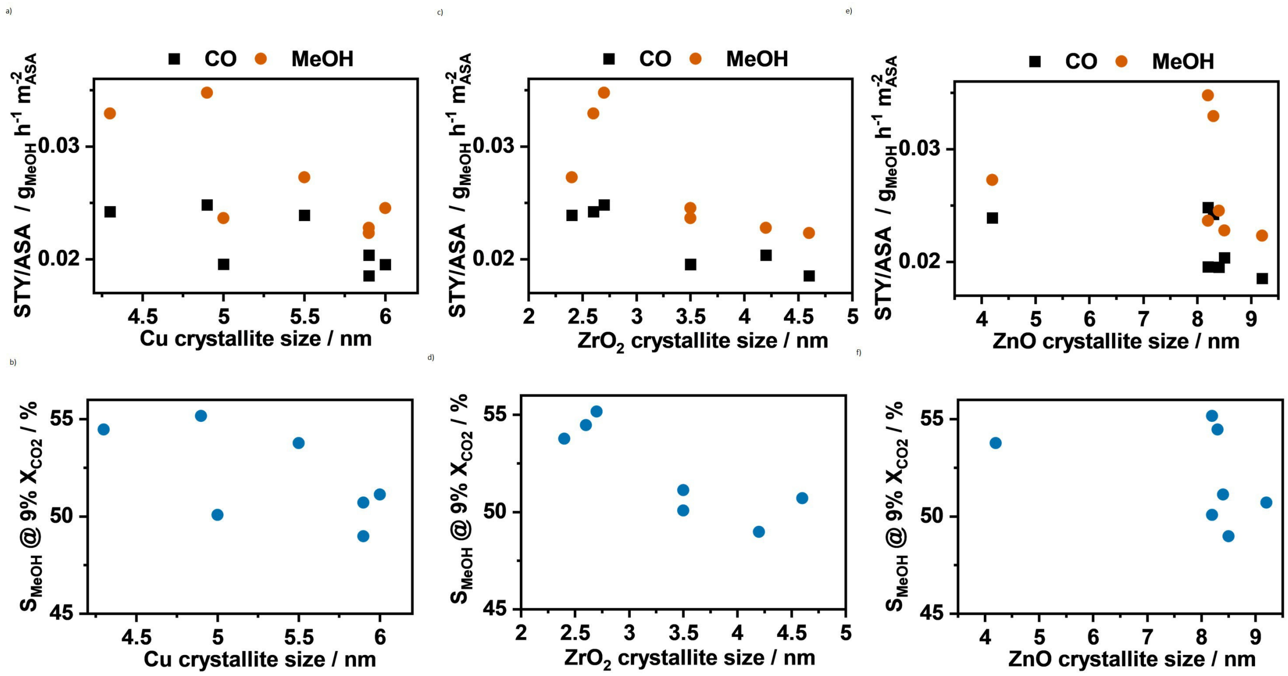

Figure 5. STY of CO and MeOH normalized to ASA obtained at 9% CO_2 conversion plotted against a) Cu crystallite size c) t-ZrO_2 crystallite size and e) ZnO crystallite size, selectivity obtained at 9% CO_2 conversion plotted against b) Cu crystallite size e) t-ZrO_2 crystallite size f) ZnO crystallite size.

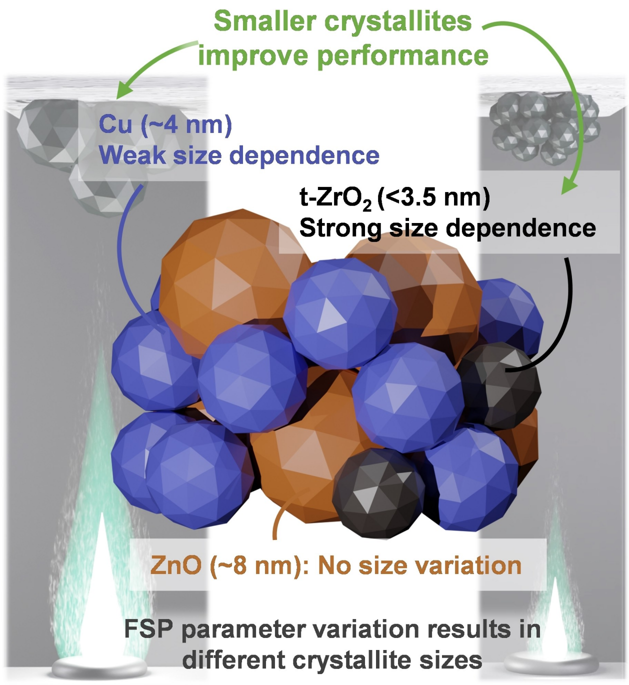

Figure 6. Schematic presentation of the influence of FSP parameter (feed rate) on the catalyst structure and the impact of the crystallite sizes of all three components of the Cu/ZnO/ZrO_2 catalyst on CO_2-to-methanol synthesis.

rather similar for all catalysts with the exception of f3-calc. For Cu and t-ZrO_2 an improvement in catalytic performance (activity + selectivity) with smaller crystallite size was observed, however, this correlation is more pronounced for t-ZrO_2 in comparison to Cu. The chosen synthesis method stirred the size of Cu and t-ZrO_2 in the same direction, therefore the less pronounced Cu dependencies might be caused by the stronger effect of t-ZrO_2. The change of STY_{MeOH} normalized to ASA with Cu and ZrO_2 size indicates that the reaction is structure-sensitive.[19]

The size effects on Cu-based catalysts and the structure-sensitivity of methanol synthesis are vividly discussed in literature. A study of Van den Berg found structure-sensitivity for particles below 8 nm for Cu particles on carbon supports for CO-based MeOH synthesis.[16] The activity increased from small nanoparticles (2 nm) to 8 nm and stabilized above that size. They suggest that this can be explained by a geometrical effect. The active step-edge sites are increasing with rising particle size and reach their saturation at 8 nm. For CO_2-to-MeOH there is still an ongoing debate about the structure-sensitivity.[17] For 10 wt.% Cu/SiO_2 catalysts in the size range from 4 to 36 nm a similar trend as for Cu/C catalysts in CO-based MeOH synthesis was observed, that the activity is lower for smaller Cu particles.[18] However, it is difficult to extrapolate the behavior of supported binary systems (model systems) on more complex ternary system.

For CZZ catalysts a linear relationship of particles above 10 nm with Cu surface area and CO_2 hydrogenation activity was found by Dong and colleagues.[21c] Arena *et al.* investigated Cu nanoparticle sizes between 2 nm and 32 nm with different composition of Cu, Zn and Zr.[8a] They found an increase in activity with increasing particle size. However, the composition of Cu/Zn/Zr in their investigation is not comparable to our system. Natesakhawat *et al.* observed the opposite behavior with various CZZ catalyst partly with promoters of Ga and Y.[19]

They observed an increase in MeOH production rate with increase of Cu surface area and they further reported decreasing TOF with increasing Cu crystallite size. The abovementioned studies focused mainly on the Cu particle size. However, in this synergistic system also the other components (ZnO and ZrO_2) play an important role.

An increase in activity for smaller ZrO_2 particles was found by Fujiwara *et al.* on FSP-made Cu/ZrO_2 catalysts.[15b] The influence of the crystallinity and different ZrO_2 polymorphs was investigated by several groups.[8b,15b,27] So far, no consensus was reached of which polymorph is most active. A few studies postulate that amorphous ZrO_2 is more active due to the weaker binding of MeOH which suppresses MeOH decomposition to CO and stronger interaction with Cu (for Cu/ZrO_2 catalysts).[27b,c] At lower feed rate, we observed a decrease in crystallinity for the samples which could also further explain in addition to Cu–Zn interfacial sites the superior activity of those catalysts. The reason for the higher selectivity cannot only be explained by the higher amount of Cu–Zn synergy, since some of those sites might also be active for the reverse water gas shift reaction, depending on interaction intensity of those sites.[28] With small Cu and ZrO_2 also more Cu-ZrO_2, ZnO-ZrO_2 and Cu-ZnO-ZrO_2 sites are present in the catalyst. Especially the ZnO-ZrO_2 interface was found to be highly selective for CO_2-to-MeOH synthesis when applying ZnO-ZrO_2 solid solution catalysts in this reaction.[29] Furthermore, for those catalysts larger ZnO_x cluster in presence of ZrO_2 seem to be the reason for the high selectivity towards MeOH.[30] Our catalysts exhibit larger ZnO particles and small ZrO_2 particles which could be beneficial and might lead to the higher selectivity.

Conclusions

In this study, a series of CZZ catalysts were systematically prepared, maintaining a similar Cu/Zn/Zr ratio comparable to commercial catalysts while varying the feed rate from 3–12 mL/min during flame spray pyrolysis. FSP presents a strategy to synthesize such catalysts, with high metal content and small crystallite sizes. We found that with increasing precursor feed rate the crystallite sizes of Cu and t-ZrO_2 increased, whereas ZnO crystallite size mostly stayed similar. The variation in crystallite size across all components resulted in differences in active and overall surface area, as well as pore volume. We found an increase of CO_2 conversion from 6.8% (f12) to 9.1% (f5), alongside an increase in MeOH selectivity (at $X_{CO2} = 9\%$ for all catalysts) from 49% (f12) to 55% (f5), with decreasing feed rate. This trend further translated into augmented MeOH formation rate (STY_{MeOH} normalized to ASA). The correlation of activity (STY/ASA) and selectivity with crystallite size across all three components showed the beneficial influence of small Cu and ZrO_2 crystallites, whereas the ZnO crystallite size exhibited only a marginal influence. These findings support earlier hypotheses that CO_2-to-MeOH synthesis is a highly structure-sensitive reaction, highlighting the influence of the particle size on catalytic activity. The higher activity might be attributed to the increased exposed Cu surface area and Cu–Zn interfacial sites. Furthermore, the presence of small ZrO_2 particles lead to an increase in ZnO-ZrO_2 sites, known for their high MeOH selectivity. Our results underscore the profound impact even slight alterations in particle size can exert on that catalytic performance of industrial-like bulk CZZ. These findings guide improved catalyst design for tackling the challenges associated with hydrogenation to MeOH using CO_2 as feedstock.

Experimental Section

Catalyst Preparation

CZZ catalysts were prepared by dissolving cupric acetate monohydrate (Fluka Chemie AG, >99%), zinc acetate dihydrate (Fluka ChemieAG, >99%) and zirconium(IV) oxide 2-ethylhexanoate in mineral spirits (Alfa Aesar, 6% Zr) in a 1:1 volumetric mixture of MeOH (Merck, >99.8%) and 2-ethylhexanoic acid (EHA, Fluka Chemie AG, >98%) (exact amounts in Table S1, ESI). The total metal concentration of the solution was 0.2 mol/L with a metal ratio of 60% Cu, 30% Zn and 10% Zr. First, the zinc precursor was dissolved in MeOH, then Cu and Zr precursors as well as EHA were added. A complete solvation of the solids was achieved by using an ultrasonic bath (1 h). The precursor solution was fed with a syringe pump (Legato210, KD Scientific) at flow rates of 3, 5, 8, and 12 mL/min through a single nozzle into a premixed flame of CH_4 (0.75 L/min) and O_2 (1.6 L/min) with a 5 L/min O_2 dispersion flow (3 bar). The setup was designed according to Mädler and Pratsinis.[31] A fiberglass filter (Whatman GF 6, d = 240 mm, Cytiva Europe GmbH) was placed in ≈50 cm distance before the lid in the combustion chamber to collect the catalyst powder by using a vacuum pump (Busch GmbH, R5). The cylinder lid was cooled with water during operation. The obtained powders were removed by scraping the filters with a spatula and sieved (≤250 μm) to remove filter residues. One half of each catalyst sprayed at a specific flow rate was subsequently calcined under static air at 300 °C for 4 h with a 5 °C/min heating ramp. The catalysts are named according to the used feed rate and calcination state *e.g.* f8 was sprayed at 8 mL/min without calcination and f12-calc was sprayed with 12 mL/min and calcined at 300 °C, respectively. The catalysts are named indicating the value of the used feed rate and calcination treatment.

Catalyst Characterization

The composition of the prepared catalysts (Cu, Zn, Zr) was measured with inductively coupled plasma-optical emission spectroscopy (ICP-OES) using an Agilent 725 spectrometer with a plasma excitation of 40 MHz and 2 kW. The samples were dissolved in a solution of hydrofluoric acid, nitric acid, and hydrochloric acid under microwave irradiation of 600 W for 90 min in an Anton Paar Multiwave 3000. For each catalyst two samples were analyzed and the average value calculated.

With thermogravimetry analysis (TGA) the presence of organic residues was investigated. Therefore, the samples were placed on a crucible and heated in static synthetic air (Air Liquide, Alphagaz 1) from 25 °C to 800 °C with a 5 °C/min ramp using a Mettler Toledo TGA2 LF/1100/833 apparatus.

Crystalline phases and crystallite sizes of the fresh, calcined, and reduced catalyst were analyzed by X-Ray powder diffraction using a PANalytical X'Pert PRO diffractometer with Cu Kα radiation ($\lambda = 1.5406$ Å) with a Ni filter. Diffraction patterns were recorded from $2\theta = 20°$ to 80° in 0.625° steps with 8 min/step. The patterns were analyzed with the X'Pert HighScore software and Rietveld refinements[32] were performed with Topas software (v.6, Bruker AXS).[33] A LaB_6 NIST 640b standard was used for the instrumental profile, using a pseudo-Voigt Thompson-Cox Hasting peak shape. The microstructure analysis was performed using double-Voigt approach by Balzar implemented in Topas to derive crystallite size and strain.[34] For CuO the structure of Asbrink *et al.*[35] was used, for the Cu phase the structure from Shkvarina *et al.*,[36] for the ZnO phase the structure of Kisi *et al.*[37] and for t-ZrO_2 the structure from Bondars *et al.*[38]

The specific surface area of the catalysts was determined by N_2-physisorption at −196 °C using a BELSORP-mini II (Rubotherm) and calculated applying the Brunauer-Emmett-Teller (BET) method in the p/p_0 range of 0.05–0.3 (typically 11 points). The catalyst samples were heated for 1 h at 200 °C prior to the measurement.

The morphology of selected CZZ samples (f3, f3-calc, f5, f12) was investigated by transmission electron microscopy (TEM). The catalyst composition and metal distribution were evaluated by Scanning-TEM energy dispersive X-ray spectroscopy (STEM-EDX). The mean particle diameter was obtained by counting more than 100 particles from several bright-field TEM images with the ImageJ software.

The reduction behavior was probed with H_2 temperature programmed reduction (TPR). 50 mg of the catalyst (200–300 μm) was dried at 150 °C in Ar (50 mL/min) for 1 h and cooled to room temperature. Then the sample was heated to 300 °C with a rate of 5 °C/min while being reduced in 10% H_2 in Ar (50 mL/min). A thermal conductivity detector (TCD) measured the H_2 consumption. Data were recorded using a Micromeritics AutoChem II 2920 analyser.

Subsequently, after TPR, the active surface area (ASA) was determined with pulse N_2O titration.[39] Prior to the experiment, the surface was cleaned by flushing with He (50 mL/min) at 300 °C for 1 h and then cooled to 35 °C under He flow. 1 mL pulses of 1% N_2O in He were dosed and the outlet gas composition was analyzed with a mass spectrometer (Pfeiffer Vacuum Omnistar). The surface area calculation assumed half monolayer oxygen coverage (Cus:Oads = 2:1) and a Cu surface atom density of $6.8 \cdot 10^{-20}$ m^2/atom.[39]

Catalyst Testing

The catalytic performance was tested in a laboratory setup with a stainless steel fixed-bed tubular reactor (length 410 mm, 7 mm in inner diameter and 3/8" outer diameter) and a split tube furnace (HTM Reetz GmbH) (Scheme S1, ESI). The catalyst bed (length 3 cm) consisted of ≈0.35 g of the catalyst particles (300 μm to 450 μm) diluted in 1.05 g silicium carbide SiC (Carborundum 210 μm, VWR Chemicals) (Table S4, ESI). Above and below the catalyst bed the reactor was filled with SiC (Carborundum 500 μm, VWR Chemicals). Two thermocouples were located at the inlet and outlet of the catalyst bed for temperature control. Mass flow controllers (Bronkhorst) were used for gas dosage and an on-line micro gas chromatograph (μ-GC) (Inficon Fusion Micro GC, PoraPLOT Q, 10 m length and 0.25 mm diameter with carrier gas helium and a mole sieve column with 5 Å, 0.25 mm diameter, 10 m length and carrier gas argon) was used for gas analysis. To prevent condensation of products the gas pipes were heated to 150 °C. A flow meter (Bios DryCal definer 220 gas flow calibrator, MesaLabs) was used to calibrate the gas flows.

Prior to the catalytic test, the catalysts were reduced *in situ* at 275 °C (heating rate 5 °C/min) for 1 h in a mixture of 10% H_2 in N_2 (both Air Liquide, 99.9999%) at 1 bar. Subsequently, the reactor was cooled to reaction temperature of 235 °C and the gas composition changed to 80% H_2/CO_2 in N_2 (Air Liquide, CO_2/N_2 mix (50:50) 99.995%, H_2 99.9999%). The reaction was carried out at three different flow rates (Table S5, ESI). CO_2 conversion, MeOH selectivity and yield, as well as space time yield (STY) and carbon balance was calculated according equations S2–S6 found in ESI.

Acknowledgements

The authors would like to thank Dr. Michael Borchers and Markus Makowiak (both Karlsruhe Institute of Technology (KIT)) for performing and supporting H_2-TPR and N_2O-Titration measurements, Marion Lenzner (KIT) for thermal gravimetric analysis, Armin Lautenbauch (KIT) for ICP-OES analysis, Angela Deutsch and Dr. Thomas Eldrigde (both KIT) for N_2 physisorption experiments (BET) and Dr. Florian Maurer (KIT) for graphical support. We thank Dr. Stephan Pitter und Dr. Anna Zimina (both KIT) for fruitful discussions on Cu/ZnO based systems and their characterization. The German Federal Ministry of Economic Affairs and Climate Action (BMWK) within the 3D-PROCESS project (03EN2065D) is gratefully acknowledged for financial support, and, in addition the DFG for financial support within the SPP2080 (GR 3987/14-2). Open Access funding enabled and organized by Projekt DEAL.

Conflict of Interests

The authors declare no conflict of interest.

Keywords: Heterogeneous catalysis · Sustainable chemistry · CO_2-to-methanol · Structure-sensitivity · Cu/ZnO/ZrO_2 catalyst

[1] V. Dieterich, A. Buttler, A. Hanel, H. Spliethoff, S. Fendt, *Energy Environ. Sci.* **2020**, *13*, 3207–3252.
[2] A. Varone, M. Ferrari, *Renew. Sustain. Energy Rev.* **2015**, *45*, 207–218.
[3] a) C. Hank, S. Gelpke, A. Schnabl, R. J. White, J. Full, N. Wiebe, T. Smolinka, A. Schaadt, H.-M. Henning, C. Hebling, *Sustainable Energy Fuels* **2018**, *2*, 1244–1261; b) G. A. Olah, A. Goeppert, G. S. Prakash, *Beyond Oil and Gas: the Methanol Economy*, Wiley-VCH Verlag GmbH & Co. KGaA, Weinheim, **2018**.
[4] A. Beck, M. A. Newton, L. G. A. van de Water, J. A. van Bokhoven, *Chem. Rev.* **2024**, *124*, 4543–4678.
[5] J. Skrzypek, M. Lachowska, M. Grzesik, J. Słoczyński, P. Nowak, *Chem. Eng. J.* **1995**, *58*, 101–108.
[6] E. Frei, A. Schaadt, T. Ludwig, H. Hillebrecht, I. Krossing, *ChemCatChem* **2014**, *6*, 1721–1730.
[7] a) B. Liang, J. Ma, X. Su, C. Yang, H. Duan, H. Zhou, S. Deng, L. Li, Y. Huang, *Ind. Eng. Chem. Res.* **2019**, *58*, 9030–9037; b) J. Wu, M. Saito, M. Takeuchi, T. Watanabe, *Appl. Catal., A* **2001**, *218*, 235–240.
[8] a) F. Arena, K. Barbera, G. Italiano, G. Bonura, L. Spadaro, F. Frusteri, *J. Catal.* **2007**, *249*, 185–194; b) X. Guo, D. Mao, G. Lu, S. Wang, G. Wu, *J. Catal.* **2010**, *271*, 178–185; c) Y. Wang, S. Kattel, W. Gao, K. Li, P. Liu, J. G. Chen, H. Wang, *Nat. Commun.* **2019**, *10*, 1166.

[9] L. Warmuth, M. Steurer, D. Schild, A. Zimina, J.-D. Grunwaldt, S. Pitter, *ACS Appl. Mater. Interfaces* **2024**, *16*, 8813–8821.
[10] A. Beck, V. Paunović, J. A. van Bokhoven, *Nat. Catal.* **2023**, *6*, 873–884.
[11] M. Behrens, R. Schlögl, *Z. Anorg. Allg. Chem.* **2013**, *639*, 2683–2695.
[12] M. Behrens, F. Studt, I. Kasatkin, S. Kuhl, M. Havecker, F. Abild-Pedersen, S. Zander, F. Girgsdies, P. Kurr, B. L. Kniep, M. Tovar, R. W. Fischer, J. K. Norskov, R. Schlögl, *Science* **2012**, *336*, 893–897.
[13] W. Y. Teoh, R. Amal, L. Mädler, *Nanoscale* **2010**, *2*, 1324.
[14] S. Liu, M. M. Mohammadi, M. T. Swihart, *Chem. Eng. J.* **2021**, *405*, 126958.
[15] a) R. Ahmad, M. Hellinger, M. Buchholz, H. Sezen, L. Gharnati, C. Wöll, J. Sauer, M. Döring, J.-D. Grunwaldt, U. Arnold, *Catal. Commun.* **2014**, *43*, 52–56; b) K. Fujiwara, S. Tada, T. Honma, H. Sasaki, M. Nishijima, R. Kikuchi, *AIChE Journal* **2019**, *65*, e16716; c) J. Jensen, T. Johannessen, S. Wedel, H. Livbjerg, *J. Catal.* **2003**, *218*, 67–77; d) S. Lee, K. Schneider, J. Schumann, A. K. Mogalicherla, P. Pfeifer, R. Dittmeyer, *Chem. Eng. Sci.* **2015**, *138*, 194–202; e) S. Polierer, S. Pitter, J.-D. Grunwaldt, D. Guse, K. Herrera Delgado, J. Jelic, M. Kind, T. N. Otto, M. Stehle, F. Studt, S. Wild, T. A. Zevaco, M. Zimmermann, 16th European Congress on Catalysis, Aachen, **2019**; f) S. Tada, K. Fujiwara, T. Yamamura, M. Nishijima, S. Uchida, R. Kikuchi, *Chem. Eng. J.* **2020**, *381*, 122750; g) S. Tada, K. Larmier, R. Büchel, C. Copéret, *Catal. Sci. Technol.* **2018**, *8*, 2056–2060; h) M. Yang, J. Yu, X. Tong, X. Sun, H. Xu, J. Sun, *Chem. Commun.* **2021**, *57*, 7509–7512; i) M. Yang, J. Yu, A. Zimina, B. B. Sarma, L. Pandit, J.-D. Grunwaldt, L. Zhang, H. Xu, J. Sun, *Angew. Chem.* **2023**, *135*, e202216803; j) J. Yu, M. Yang, J. Zhang, Q. Ge, A. Zimina, T. Pruessmann, L. Zheng, J.-D. Grunwaldt, J. Sun, *ACS Catal.* **2020**, *10*, 14694–14706; k) J. Zhu, D. Ciolca, L. Liu, A. Parastaev, N. Kosinov, E. J. M. Hensen, *ACS Catal.* **2021**, *11*, 4880–4892.
[16] R. van Den Berg, G. Prieto, G. Korpershoek, L. I. van Der Wal, A. J. van Bunningen, S. Lægsgaard-Jørgensen, P. E. de Jongh, K. P. de Jong, *Nat. Commun.* **2016**, *7*, 13057.
[17] H. Wang, J. Lu, *Chin. J. Chem.* **2020**, *38*, 1422–1444.
[18] A. Karelovic, G. Galdames, J. C. Medina, C. Yévenes, Y. Barra, R. Jiménez, *J. Catal.* **2019**, *369*, 415–426.
[19] S. Natesakhawat, J. W. Lekse, J. P. Baltrus, P. R. Ohodnicki, B. H. Howard, X. Deng, C. Matranga, *ACS Catal.* **2012**, *2*, 1667–1676.
[20] a) K. Fujiwara, S. E. Pratsinis, *AIChE Journal* **2017**, *63*, 139–146; b) R. Jossen, S. E. Pratsinis, W. J. Stark, L. Mädler, *J. Am. Ceram. Soc.* **2005**, *88*, 1388–1393.
[21] a) C. Baltes, S. Vukojevic, F. Schüth, *J. Catal.* **2008**, *258*, 334–344; b) G. Bonura, M. Cordaro, C. Cannilla, F. Arena, F. Frusteri, *Appl. Catal. B* **2014**, *152–153*, 152–161; c) X. Dong, F. Li, N. Zhao, F. Xiao, J. Wang, Y. Tan, *Appl. Catal. B* **2016**, *191*, 8–17; d) S. Polierer, D. Guse, S. Wild, K. Herrera Delgado, T. N. Otto, T. A. Zevaco, M. Kind, J. Sauer, F. Studt, S. Pitter, *Catalysts* **2020**, *10*, 816; e) J. Sloczynski, R. Grabowski, P. Olszewski, A. Kozlowska, J. Stoch, M. Lachowska, J. Skrzypek, *Appl. Catal. , A* **2006**, *310*, 127–137.
[22] a) R. Mueller, R. Jossen, S. E. Pratsinis, M. Watson, M. K. Akhtar, *J. Am. Ceram. Soc.* **2004**, *87*, 197–202; b) P. Šot, G. Noh, I. C. Weber, S. E. Pratsinis, C. Copéret, *Helv. Chim. Acta* **2022**, *105*, e202200007.
[23] S. Tada, S. Kayamori, T. Honma, H. Kamei, A. Nariyuki, K. Kon, T. Toyao, K.-I. Shimizu, S. Satokawa, *ACS Catal.* **2018**, *8*, 7809–7819.
[24] M. Shimokawabe, H. Asakawa, N. Takezawa, *Appl. Catal.* **1990**, *59*, 45–58.
[25] a) M. B. Fichtl, J. Schumann, I. Kasatkin, N. Jacobsen, M. Behrens, R. Schlögl, M. Muhler, O. Hinrichsen, *Angew. Chem. Int. Ed.* **2014**, *53*, 7043–7047; b) R. Chatterjee, S. Kuld, R. van Den Berg, A. Chen, W. Shen, J. M. Christensen, A. D. Jensen, J. Sehested, *Top. Catal.* **2019**, *62*, 649–659.
[26] D. Hochfilzer, I. Chorkendorff, J. Kibsgaard, *ACS Energy Lett.* **2023**, *8*, 1607–1612.
[27] a) K. T. Jung, A. T. Bell, *Catal. Lett.* **2002**, *80*, 63–68; b) S. Tada, A. Katagiri, K. Kiyota, T. Honma, H. Kamei, A. Nariyuki, S. Uchida, S. Satokawa, *J. Phys. Chem. C* **2018**, *122*, 5430–5442; c) F. C. F. Marcos, R. S. Alvim, L. Lin, L. E. Betancourt, D. D. Petrolini, S. D. Senanayake, R. M. B. Alves, J. M. Assaf, J. A. Rodriguez, R. Giudici, E. M. Assaf, *Chem. Eng. J.* **2023**, *452*, 139519; d) F. C. F. Marcos, F. M. Cavalcanti, D. D. Petrolini, L. Lin, L. E. Betancourt, S. D. Senanayake, J. A. Rodriguez, J. M. Assaf, R. Giudici, E. M. Assaf, *Chem. Eng. J.* **2022**, *427*, 130947.
[28] a) J. Wen, C. Huang, Y. Sun, L. Liang, Y. Zhang, Y. Zhang, M. Fu, J. Wu, L. Chen, D. Ye, *Catalysts* **2020**, *10*, 533; b) C. Álvarez Galván, J. Schumann, M. Behrens, J. L. G. Fierro, R. Schlögl, E. Frei, *Appl. Catal. B* **2016**, *195*, 104–111; c) S. Saedy, M. A. Newton, M. Zabilskiy, J. H. Lee, F. Krumeich, M. Ranocchiari, J. A. van Bokhoven, *Catal. Sci. Technol.* **2022**, *12*, 2703–2716.
[29] J. Wang, G. Li, Z. Li, C. Tang, Z. Feng, H. An, H. Liu, T. Liu, C. Li, *Sci. Adv.* **2017**, *3*, e1701290.
[30] X. Zhang, G. Zhang, X. Zhou, Z. Wang, Y. Liu, J. Zhu, C. Song, X. Guo, *Ind. Eng. Chem. Res.* **2023**, *62*, 21173–21181.
[31] a) L. Mädler, H. K. Kammler, R. Mueller, S. E. Pratsinis, *J. Aerosol Sci* **2002**, *33*, 369–389. b) R. Mueller, L. Mädler, S. E. Pratsinis, *Chem. Eng. Sci.* **2003**, *58*, 1969–1976.
[32] a) H. M. Rietveld, *Acta Crystallogr.* **1967**, *22*, 151–152; b) H. M. Rietveld, *J. Appl. Crystallogr.* **1969**, *2*, 65–71.
[33] DIFFRAC.SUITE TOPAS - XRD Software Bruker, https://www.bruker.com/de/products/x-ray-diffraction-and-elemental-analysis/x-ray-diffraction/xrd-software/topas.html.
[34] D. Balzar, *Int. Union Crystallogr. Monogr. Crystallogr.* **1999**, *10*, 94–126.
[35] S. Åsbrink, L. J. Norrby, *Acta Cryst. B* **1970**, *26*, 8–15.
[36] E. G. Shkvarina, A. A. Titov, A. S. Shkvarin, J. R. Plaisier, L. Gigli, A. N. Titov, *Acta Cryst. C* **2018**, *74*, 1020–1025.
[37] E. H. Kisi, M. M. Elcombe, *Acta Cryst. C* **1989**, *45*, 1867–1870.
[38] B. Bondars, G. Heidemane, J. Grabis, K. Laschke, H. Boysen, J. Schneider, F. Frey, *J. Mater. Sci.* **1995**, *30*, 1621–1625.
[39] O. Hinrichsen, T. Genger, M. Muhler, *Chem. Eng. Technol.* **2000**, *23*, 956–959.